JACS
JOURNAL OF THE AMERICAN CHEMICAL SOCIETY

ARTICLE

pubs.acs.org/JACS

Spectroelectrochemical Investigation of Intramolecular and Interfacial Electron-Transfer Rates Reveals Differences Between Nitrite Reductase at Rest and During Turnover

Łukasz Krzemiński,[†] Lionel Ndamba,[§] Gerard W. Canters,[§] Thijs J. Aartsma,[§] Stephen D. Evans,[‡] and Lars J. C. Jeuken*[,†]

[†]Institute of Membrane and Systems Biology and [‡]School of Physics and Astronomy, University of Leeds, Woodhouse Lane, Leeds LS2 9JT, United Kingdom

[§]Leiden Institute of Physics, Leiden University, P.O. Box 9504, 2300 RA, Leiden, The Netherlands

Supporting Information

ABSTRACT: A combined fluorescence and electrochemical method is described that is used to simultaneously monitor the type-1 copper oxidation state and the nitrite turnover rate of a nitrite reductase (NiR) from *Alcaligenes faecalis* S-6. The catalytic activity of NiR is measured electrochemically by exploiting a direct electron transfer to fluorescently labeled enzyme molecules immobilized on modified gold electrodes, whereas the redox state of the type-1 copper site is determined from fluorescence intensity changes caused by Förster resonance energy transfer (FRET) between a fluorophore attached to NiR and its type-1 copper site. The homotrimeric structure of the enzyme is reflected in heterogeneous interfacial electron-transfer kinetics with two monomers having a 25-fold slower kinetics than the third monomer. The intramolecular electron-transfer rate between the type-1 and type-2 copper site changes at high nitrite concentration ($\geq$520 μM), resulting in an inhibition effect at low pH and a catalytic gain in enzyme activity at high pH. We propose that the intramolecular rate is significantly reduced in turnover conditions compared to the enzyme at rest, with an exception at low pH/nitrite conditions. This effect is attributed to slower reduction rate of type-2 copper center due to a rate-limiting protonation step of residues in the enzyme's active site, gating the intramolecular electron transfer.

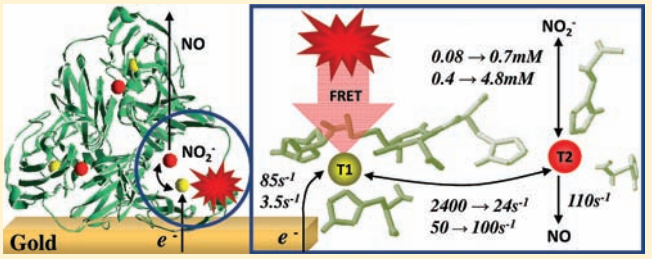

INTRODUCTION

Copper-containing nitrite reductase (NiR) catalyzes an one-electron reduction of nitrite to nitric oxide: $NO_2^- + 2H^+ + e^- \rightarrow NO + H_2O$ in denitrifying organisms.[1] NiR is a homotrimer, in which each subunit contains a type-1 and a type-2 copper site (Figure 1).[2,3] The type-1 Cu site, which is located close to the protein's surface, accepts electrons from its natural donor, pseudoazurin, and transfers them to the buried type-2 Cu site where nitrite is reduced.[2,4−9] In the type-1 copper center of green NiR from *Alcaligenes faecalis*, the copper atom is coordinated by two histidines, one methionine, and one cysteine.[10] A ligand-to-metal charge transfer (LMCT) from the sulfur (cysteine) to the oxidized copper (Cu^{2+}) gives rise to absorption bands around 450 and 590 nm, which disappear when the copper gets reduced (Cu^{1+}). In contrast, the type-2 copper center is referred to as a nonblue copper site (its visible absorption spectrum is neglectable compared to that of the type-1 copper site) and is coordinated by three histidine residues, with a fourth position occupied by one of the following ligands: H_2O, OH^-, or NO_2^-.[10−13] The reduction of this site may also lead to its isomerization into an inactive reduced state, in which the fourth ligand is lost.[8] The type-2 Cu site, together with a water network around an aspartate and a histidine residue, forms the active site of the enzyme.[8,9,11,14,15]

The catalytic cycle of NiR has been under the extensive debate for the past decade, in which the question "What happens first in the type-2 copper site, nitrite binding or reduction of the metal?" has been a central point. Historically, the first discussions revolved around the ordered (single-route) mechanisms, in which it was assumed that nitrite only binds to the reduced site (reduction before binding route, route A)[16−19] or, alternatively, that the nitrite only binds to the oxidized site (binding before reduction route, route B).[1,10,20,21] More recently, Wijma et al. have studied NiR with kinetic techniques and protein-film voltammetry (PFV) and proposed a random sequential mechanism (RSM) in which both routes contribute to NiR's catalytic cycle with the contribution of each route depending on pH and nitrite concentration.[8,9] It was hypothesized that the enzyme's homotrimeric structure leads to dispersion in interfacial

Received: May 27, 2011
Published: August 24, 2011

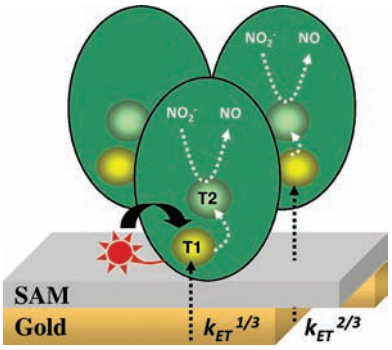

Figure 1. A schematic representation of a SAM modified gold electrode with fluorescently labeled, copper-containing L93C NiR on top. The bold arrow signifies the quenching of the fluorescent dye (red star) through FRET to the type-1 site (yellow). The dashed arrows illustrate the ET process from the electrode surface via type-1 Cu to type-2 Cu site (green), where the nitrite reduction to nitric oxide takes place. In this schematic representation, one of the monomers (1/3) is closer to the electrode than the other two (2/3). Therefore, two interfacial ET rates ($k_{ET}^{1/3}$ and $k_{ET}^{2/3}$) are distinguished.

electron-transfer (ET) rates when NiR is adsorbed on carbon electrodes. Crucially, in PFV, distinguishing between interfacial and intramolecular ET relies on varying the electrode potential as only the interfacial ET is dependent on the potential. This can lead to complex models, especially when multiple catalytic routes and heterogenic interfacial ET need to be accounted for.

To obtain a more direct proof of the catalytic cycle of NiR and to increase our insight, we have combined the PFV technique with a novel fluorescent method, called FluRedox, that directly reports on the redox state of the type-1 copper site.[22−25] The method works on the basis of Förster resonance energy transfer (FRET), in which the emission of a suitable fluorophore (positioned close to the type-1 copper site) is diminished when the site is oxidized. This technique has been previously used to study NiR at the single-molecule level.[22] Recently, it was shown that FluRedox can be combined with electrochemistry, and initial experiments with a small ET protein, azurin, revealed kinetic and thermodynamic heterogeneity when this protein is adsorbed on gold electrodes.[24] Here, we have adopted this method to the study of NiR with the aim to determine the oxidation state of the type-1 Cu site during turnover. The fluorescence intensity changes are measured with an epi-fluorescence microscope, while the redox state and turnover rate of the enzyme are controlled electrochemically. Here, we show how the oxidation state of the type-1 copper correlates with turnover kinetics at the type-2 copper site. Moreover, kinetic constants at low (5.45) and high (6.85) pH are determined for the RSM in NiR. The intramolecular ET rate between the type-1 and type-2 copper site is dependent on pH. In addition, the magnitude of this ET rate is found to differ for NiR at rest and during turnover. Finally, heterogeneity in the interfacial ET rate between modified gold and the type-1 copper is suggested to be related to the homotrimeric structure of NiR.

METHODS

General. Apart from protein labeling, all experiments were performed in either 20 mM of 4-morpholine propane sulfonic acid (MOPS) (Sigma) pH 6.85 or 20 mM of 2-(*N*-morpholino)ethanesulfonic acid (MES) (Sigma) pH 5.45 together with 30 mM of Na_2SO_4 (Sigma) as a supporting electrolyte. The buffers, as well as all cleaning solutions, were prepared using ultrapure Milli-Q (Millipore) water of 18.2 M $\Omega \cdot cm^2$, whereas thiol solutions were made in isopropanol (HPLC grade, Fluka). All potentials are quoted versus silver/silver chloride (Ag/AgCl, sat. KCl) reference electrode (Radiometer) with Ag/AgCl being 199 mV vs the normal hydrogen electrode (NHE).

Protein Labeling. The Cu L93C NiR (from *A. faecalis* S-6) was expressed and purified as described previously.[26] The Zn L93C variant of NiR was prepared using the same protocol with modifications as follows: *Escherichia coli* bacteria were grown on yeast extract and tryptone (YT) medium with addition of 0.5 mM of $ZnCl_2$, while 1 mM of $ZnCl_2$ (instead of 1 mM of $CuCl_2$) was introduced after the cell lysis. The copper and zinc content of the enzymes used for electrode experiments was 1.4 Cu/0.4 Zn per monomer of Cu L93C NiR and 0.01 Cu/2.2 Zn per monomer of Zn L93C NiR, as determined from atomic absorption spectroscopy. Prior to labeling, 200 μM of L93C NiR (monomer) was reduced with 20× molar excess of reducing agent, Tris(2-carboxyethyl)phosphine (TCEP, Sigma), in order to break disulfide bonds that might have formed between L93C NiR trimers. Next, the reduced protein was passed through Centri-Spin 10 size exclusion chromatography spin columns with 5 kDa cutoff (Princeton Separations) in order to remove TCEP. Following this, a 3-fold excess (Cu L93C) or half (Zn L93C) of ATTO 565 maleimide (ATTO-TEC GmbH, this dye is positively charged after conjugation) over 100 μM of protein monomer was used to label L93C NiR, after which free label was removed by gel filtration (Centri-Spin 10 columns).[23,25] The labeling reaction was performed in *N*-(2-hydroxyethyl)piperazine-*N*′-ethanesulfonic acid (HEPES) buffer at pH 7.3 (Sigma). The efficiency of the labeling was quantified spectroscopically using $\varepsilon_{565} = 120\ mM^{-1} \cdot cm^{-1}$ for ATTO 565 and $\varepsilon_{280} = 46\ mM^{-1} \cdot cm^{-1}$ per monomer for the Cu and Zn variants of NiR.[26] The labeling conditions were chosen to yield (on average) no more than one dye molecule per enzyme trimer (26−28% monomers labeled). The fluorescence measurements in bulk were conducted as previously described[22,23,25] and showed a FRET efficiency (ATTO 565 to the type-1 copper site) of 50−60%.

Electrode Modifications and Spectroelectrochemistry Experiments. All experiments were carried out with template stripped gold (TSG) working electrodes, prepared as described previously.[27,28] Self-assembled monolayers (SAM) were made by incubating the TSG slide with 1.5 mM of 6-mercapto-hexanol (6-MH, Sigma) for 5 h. After this time, the excess of thiols was removed using isopropanol and methanol; the electrodes were dried with N_2 and further incubated with 3 μM (monomer) of ATTO 565 labeled Cu L93C NiR or Zn L93C NiR for 20 min. Directly after this, the enzyme modified electrodes were rinsed three times with water or buffer and used in the spectroelectrochemistry experiments.

A home-built spectro-electrochemical cell (see Figure 8, Supporting Information) was used in which a flow cell of all-Teflon construction houses the gold working electrode (via a rubber O-ring, electrode area = 0.18 cm^2), a platinum wire counter electrode, and a saturated silver/silver chloride electrode (Ag/AgCl). The reference electrode is fitted through a side connector that places it at about 4 cm distance from the gold working electrode. The flow cell is closed with a glass coverslip, which allows for epi-fluorescence measurements. All buffers used in the flow cell were deoxygenated (1 h of Ar purging before the experiment start) and kept under vigorous Argon flux during the experiment. A Chi604c potentiostat was used to measure cyclic voltammograms (CVs, 10 mV/s, potential window of +300 to −400 mV vs Ag/AgCl) and chronoamperograms (a single potential of −200 mV vs Ag/AgCl). A Nikon i90 epi-fluorescent microscope, equipped with a Hamamatsu C4742-96-12G04 camera, was used to measure the fluorescence intensity change. The microscope settings were as follows: excitation band-pass filter, 530−560 nm; dichroic mirror, 570 nm; emission band-pass filter, 590−650 nm; and 1 s exposure time. The fluorescence background

(~250 arbitrary units [A.U.]) was determined from the electrode modified with unlabeled enzyme and was subtracted from all data.

The electroactive coverage of the enzyme was determined using the area of the baseline-subtracted signals from CVs measured at a scan rate (v) of 10 mV/s of labeled NiR on 6-MH modified gold, in the absence of nitrite. The baseline was subtracted using SOAS software, freely available from Dr. C. Léger,[29] and the coverage calculated with $\text{area}/v = nFA\Gamma$, in which A is the surface area of the electrode, Γ is the enzyme coverage, F is the Faraday constant, and n is the number of electrons per monomer of NiR ($n = 2$). The catalytic current, i_{cat}, was converted into the catalytic rate k_{cat} according to $i_{cat} = -FA\Gamma k_{cat}$, in which the negative sign stands for reduction reaction.

Nonspecific Fluorescence Changes. As explained in the Results Section, at pH 6.85 we have to correct for nonspecific fluorophore emission changes due to the potential-driven reorganization of labeled NiR molecules on the electrode. This phenomenon was previously encountered for azurin.[24] The unspecific contribution to the overall fluorescence intensity (F_i) is distinguished from specific FRET changes (due to redox changes of the type-1 copper site) by comparing the copper- and zinc-containing L93C NiR samples in the first 300 s after applying a potential at −200 mV vs Ag/AgCl. As the two processes undergo different kinetics, it was possible to distinguish them by fitting the trace to single and double exponentials. The F_i change of labeled Cu-NiR was fitted to a double exponential, whereas the F_i increase from labeled Zn-NiR was fitted to a single exponential. The extracted parameters revealed similar fluorescence kinetics and amplitude of the Zn-NiR sample (A = 97.0 A.U., k = 0.019 s^{-1}) compared to the slow component of the Cu-NiR samples (A = 97.5 A.U., k = 0.015 s^{-1}). The fast component of the Cu-NiR sample (A = 259.5 A.U., k = 0.098 s^{-1}) was assumed to be due to the FRET-detected reduction of the NiR. Therefore we corrected for nonspecific fluorescence changes of labeled Cu-NiR by subtracting the fluorescence amplitude of the slow phase.

Model. The experimental results were analyzed on the basis of the model shown in Figure 7. The model assumes that at low nitrite concentrations, the type-2 copper site is coordinated by water (pH 5.45) or a hydroxyl ion (pH 6.85), which is replaced by nitrite at high nitrite concentrations.[8,9] The model we used is conceptually based on Wijma et al.'s previous proposed RSM of NiR.[8,9] According to the RSM, during the catalytic cycle, the type-2 Cu site can be reduced before (route A) or after binding of NO_2^- (route B). In Figure 7, the possibility that the type-1 Cu site is either reduced or oxidized is included, doubling (as compared to previously employed schemes)[8,9] the possible oxidation states of NiR during turnover (from 4 to 8). Instead of the traditional K_m and V_{max} kinetic values characterizing NiR catalysis, Figure 7 defines a set of ET rates and binding constants. The main assumption, justified by the high overpotential used (−200 mV vs Ag/AgCl), is that the interfacial ET (k_{ET}) proceeds only in one direction, from the gold electrode to the enzyme's type-1 Cu site. Similarly, the final catalytic step (k_3) is equal for both routes (A and B). Furthermore, in line with standard Henri−Michaelis−Menten (HMM) analysis, the on- and the off-rates for NO_2^- binding to the active site are assumed to be fast compared to turnover rates, and thus the enzyme−substrate complex is characterized by dissociation constants (K_D^A, K_D^B). Finally, we assume that the substrate binding constants are not affected by the oxidation state of type-1 Cu site.

Taking the steady-state conditions, $\delta[X]/\delta t = 0$, where $[X]$ is the concentration of the consecutive enzyme state [A], ..., [H], each state can be expressed as a function of the ET rates and dissociation constants. The fluorescence intensity (F_i) can be calculated as $F_i = ([B] + [D] + [F] + [H])/\Gamma$ as well as catalytic turnover $k_{cat} = k_3([E] + [F])/\Gamma$ (see Supporting Information), where Γ stands for the sum of all stages ([A] +, ..., + [H]). Under steady-state conditions, the interfacial ET must equal turnover rate and thus $k_{cat} = k_{ET}([A] + [C] + [E] + [G])/\Gamma = -k_{ET}([B] + [D] + [F] + [H])/\Gamma$. Importantly, it thus follows that under steady-state conditions $F_i/k_{cat} = -1/k_{ET}$. We note that this is independent of the details of the model shown in Figure 7 and also applies to simpler models. Equations for [A], ..., [H], F_i and k_{cat} were solved using Maple 13 software and a determinant method.[30] The model implies that the minimum fluorescence level obtained during the titration with nitrite has to be >0, whereas the maximum is 1 (fully reduced type-1 Cu site).

RESULTS

Cyclic Voltammetry. The effect of various gold electrode modifications on NiR enzyme activity will be described elsewhere. Here, the ATTO 565 labeled L93C Cu-NiR enzyme was found to be active on 6-mercapto-hexanol (6-MH) modified gold. In the absence of nitrite, reduction and oxidation, peaks (at 0 ± 10 and 78 ± 10 mV vs Ag/AgCl, respectively; Figure 2A, solid black line) are observed with reduction potentials in good agreement with the literature.[8,26,31,32] No voltammetric features are detected with the zinc variant of the adsorbed NiR. Using the area underneath the redox peaks (see Methods Section), the electroactive coverage of the enzyme was determined and found to vary between 1.66−1.85 pmol/cm^2 (equivalent to 16−18% of a closely packed monolayer). In the presence of nitrite, a strong catalytic current (i_{cat}) is observed as the electrode potential is taken below 0 V vs Ag/AgCl (Figure 2B, solid black line). This current increases gradually when the electrode potential is lowered, suggesting dispersion of the intermolecular ET rate,[33,34]

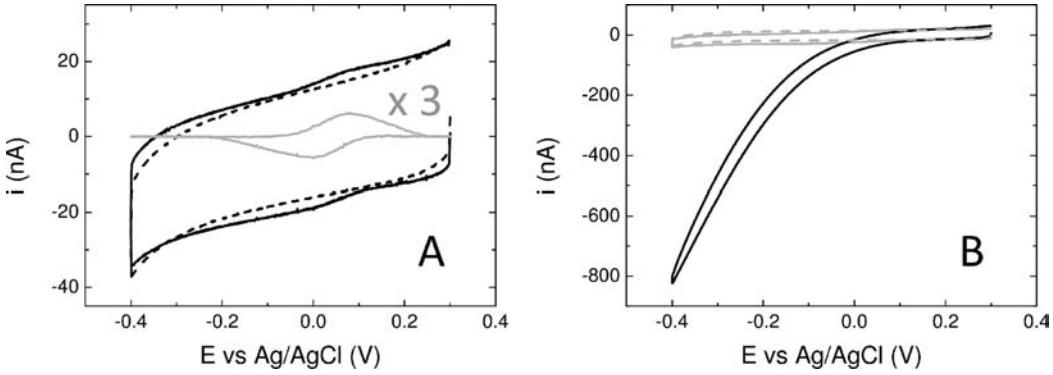

Figure 2. (A) CV before (dashed black line, baseline) and after (solid black line) adsorption of ATTO 565 labeled L93C Cu-NiR onto 6-MH gold electrode, together with baseline-subtracted protein signal (gray line). The baseline-subtracted signal is amplified three times for clarity. (B) CV recorded from ATTO 565 labeled L93C Cu-NiR adsorbed on 6MH-gold in absence (solid gray line) or presence (solid black line) of nitrite (40 mM) and ATTO 565 labeled L93C Zn-NiR (dashed gray line) adsorbed on 6-MH gold, in presence of nitrite (40 mM). All scans were taken at 10 m V/s, pH = 6.85.

similar to previous studies of NiR adsorbed on graphite electrodes.[8,9] Again, no catalytic current is observed with the zinc variant of NiR (Figure 2B, dashed gray line).

Spectroelectrochemistry at pH 5.45. Figure 3 shows a typical spectroelectrochemistry experiment for ATTO 565 labeled L93C Cu-NiR at pH 5.45. When −200 mV vs Ag/AgCl potential is applied, a rapid increase of the fluorescence intensity (F_i) is observed (Figure 3, black line). F_i is a direct measure of the oxidation state of Cu-NiR's type-1 Cu center (reduction of the type-1 Cu site diminishes FRET and thus increases the fluorescence intensity of ATTO 565). When nitrite is added in a stepwise manner (Figure 3, numbers 1−11), a gradual decrease in F_i is observed (type-1 copper sites oxidize). At the same time, the catalytic current (i_{cat}) increases (Figure 3, gray line) due to NO_2^- reduction by the enzyme. When the nitrite concentration is raised above 520 μM, substrate inhibition decreases the activity of NiR. Wijma et al. have previously reported this effect at low pH.[8,9] When the inactive zinc variant of NiR is used, no changes are observed in either F_i or i_{cat} when a potential is applied or nitrite is added.

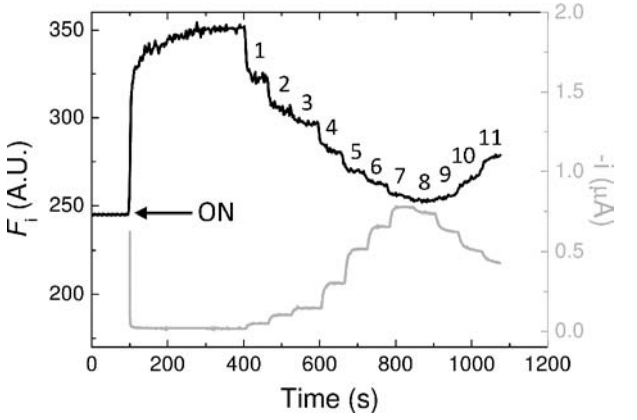

Figure 3. An example of spectroelectrochemistry data collected from ATTO 565 labeled L93C Cu-NiR activity titration on a 6-MH modified gold electrode, at pH 5.45. The reductive current ($-i = i_{cat}$) time traces are represented by gray line/axis (chronoamperogram), whereas the FRET-based fluorescence changes are given by a black line/axis; −200 mV (vs Ag/AgCl) is applied to the enzyme modified electrode after 100 s (ON), then after another 300 s, nitrite is subsequently added (400−1100 s). The numbers stand for following nitrite concentrations: 1 = 1 μM, 2 = 2.5 μM, 3 = 5 μM, 4 = 15 μM, 5 = 50 μM, 6 = 120 μM, 7 = 520 μM, 8 = 2.52 mM, 9 = 7.52 mM, 10 = 17.5 mM, 11 = 27.5 mM.

Spectroelectrochemistry at pH 6.85. In contrast to the results obtained at pH 5.45, the F_i response was found to be affected by electric-field effects at pH 6.85. The experiment conducted on the zinc variant of ATTO 565 labeled NiR (Figure 4B) reveals a nonspecific F_i increase when −200 mV vs Ag/AgCl is applied. This potential-driven effect is ascribed to protein reorganization on the surface, resulting in a change in distance between the metal surface and the fluorophore. This will affect the metal-based quenching.[35−37] For pH 6.85, the data obtained with Zn-NiR were used to correct those of Cu-NiR (see Methods Section). Another difference between low (5.45) and high (6.85) pH is apparent during the enzyme's titration with nitrite. Figure 4A shows no substrate inhibition is observed for nitrite concentrations studied here. Finally, the enzyme is more active at lower pH (Figures 3 and 4A, gray lines), again in agreement with literature reports.[5,8,11]

Surprisingly, the fluorescence signal of the labeled NiR, immobilized on the electrode, is found to be relatively insensitive to photobleaching (Figure 4B, black line). This fact we attribute to an electrode-based quenching mechanism that protects against the fluorophore's photodestruction, a phenomenon predicted by theory[38] and seen experimentally.[39] The redox system operating under experimental conditions may also speed up the rate of triplet-state depopulation of ATTO 565 into the electronic ground state, thus enabling fluorophore's recovery rather than photobleaching.[40] In separate experiments, we observed that when labeled protein is placed at larger distances from gold interface (30−50 nm), the fluorescent signal is about 20 times as intense but strongly affected by photobleaching. The fact that photobleaching is almost absent for the 6-MH modified gold electrodes used here enables us to accurately and quantitatively measure the fluorescence intensity for prolonged periods.

Interfacial Electron Transfer. It can be shown that a homogeneous enzyme electrode will produce a linear relationship between F_i and k_{cat}, with a slope of $-1/k_{ET}$ (see Model Section in Methods). This relationship is a consequence of the fact that under steady-state conditions the interfacial ET (reducing the type-1 copper site) is equal to the turnover rate. As this latter statement is independent of the model used, the relationship holds irrespectively of the model. However, Figure 5 explicitly shows a deviation from this relationship (dashed red lines) and

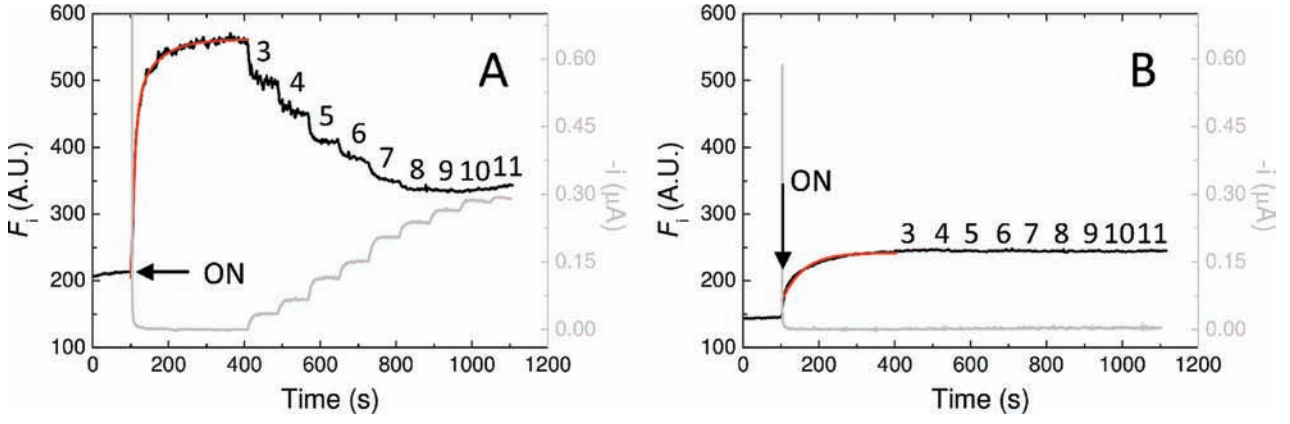

Figure 4. An example of spectroelectrochemistry data collected from ATTO 565 labeled L93C Cu-NiR (A) and L93C Zn-NiR (B) on 6-MH modified gold electrodes, at pH 6.85. The experimental conditions are the same as for Figure 3. The red lines are the fits to double-exponential (A) and single-exponential (B) equations (see Methods Section). The numbers stand for nitrite concentrations, as described in the legend of Figure 3.

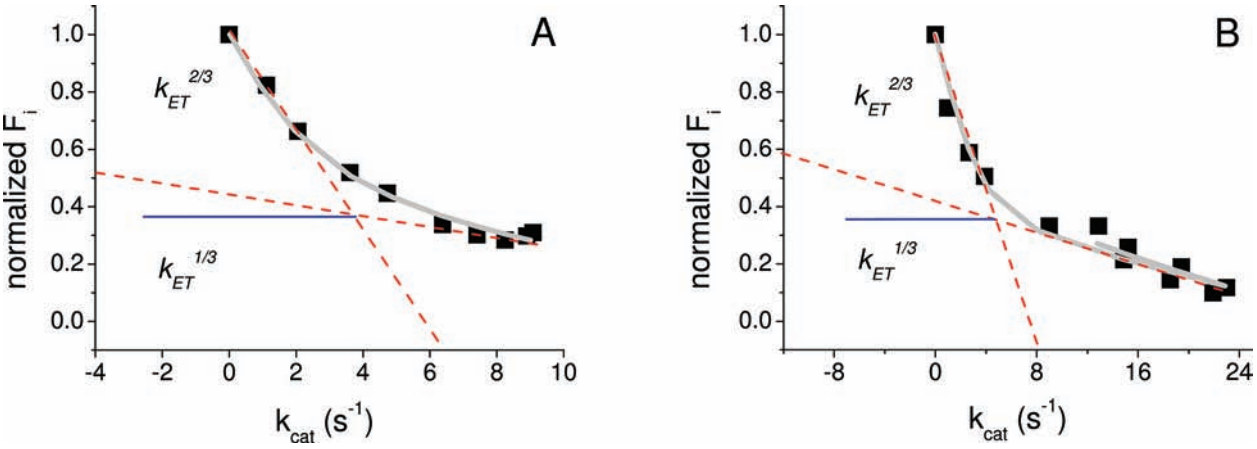

Figure 5. Deviations from a single interfacial ET rate (red dashed lines) illustrating heterogeneity in the ET rate to ATTO 565 labeled L93C Cu-NiR. The normalized fluorescence is plotted against the catalytic activity at pH 6.85 (A) and pH 5.45 (B). The filled squares represent F_i and k_{cat} values for subsequent concentrations of nitrite (1−11 as in Figure 3). The data are fitted (gray lines) to our model (see Methods Section and Figure 7) with two interfacial ET rates (k_{ET}) assumed. Analysis of dash red lines reveals the approximate values of $k_{ET}^{1/3}$ and $k_{ET}^{2/3}$ at both pH values (see text).

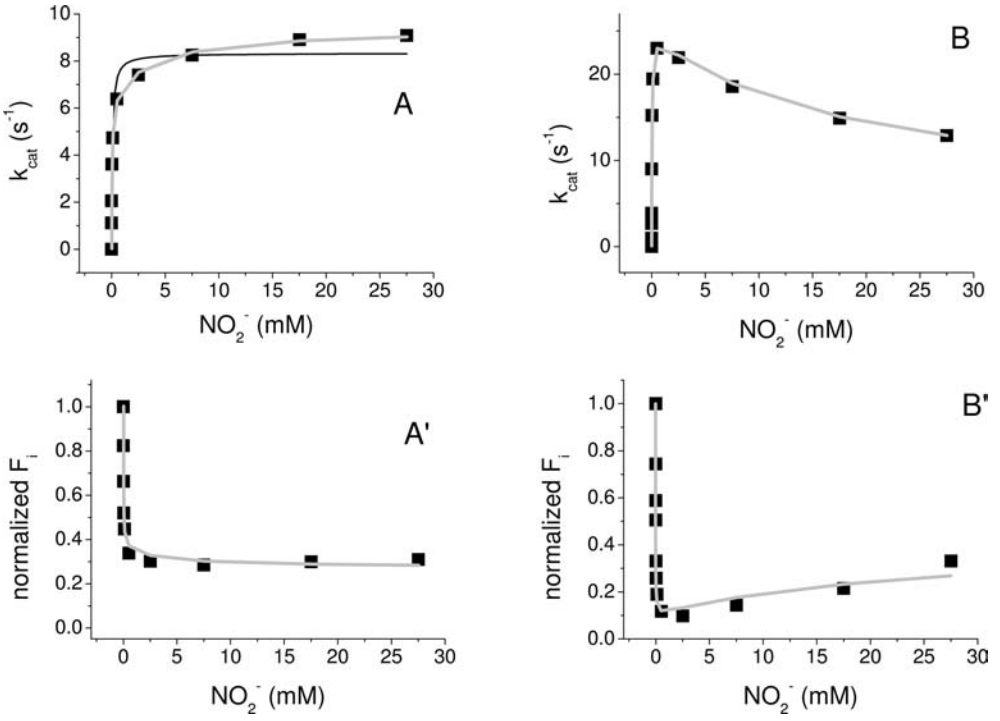

Figure 6. Example fits to spectroelectrochemistry data collected at pH 6.85 (Figure 4A; A, A′ here) and pH 5.45 (Figure 3; B,B′ here). Both signals, enzyme's catalytic activity (A, B), and FRET-depended ATTO 565 normalized fluorescence change (A′, B′) are plotted (filled squares) against nitrite concentration (1−11 as in Figure 3) and fitted into our model (gray lines). The black line on graph A represents the enzymes activity fitted into HMM equation. The data were fitted with two interfacial ET rates ($k_{ET}^{1/3}$ and $k_{ET}^{2/3}$, see Figure 5).

directly indicates that at least two electrode−enzyme interfacial ET rates are present. Figure 5 is thus indicative of enzyme heterogeneity on the surface and gives us a rough estimate of the enzyme subpopulations and the ET rates. The slope analysis of the dashed red lines suggests two subpopulations. The intercept of the two dashed lines in Figure 5 occurs at $F_i \approx 0.35$, corresponding to a 2 to 1 ratio (i.e., 0.66 to 0.33 ratio). Taking the slope to be equal to $-1/k_{ET}$, k_{ET} for the two subpopulations can be estimated to be 6 and 70 s^{-1} at pH 6.85 and 7 and 95 s^{-1} at pH 5.45.

Data Fitting. Figure 6 shows an example of the steady-state catalytic rate, k_{cat} (related to i_{cat}, see Methods Section), and the fluorescence intensity, F_i, levels as a function of nitrite concentration. These data are fitted to the model shown in Figure 7, and the fits are shown by the gray lines in Figure 6. Data of three different experiments conducted at each pH are analyzed independently and used to calculate the standard error of the mean (S.E.M.) for the parameters given in Table 1. Analysis indicates that multiple solutions can be found when fitting the data (most of them with physiological unrealistic values) and at least one

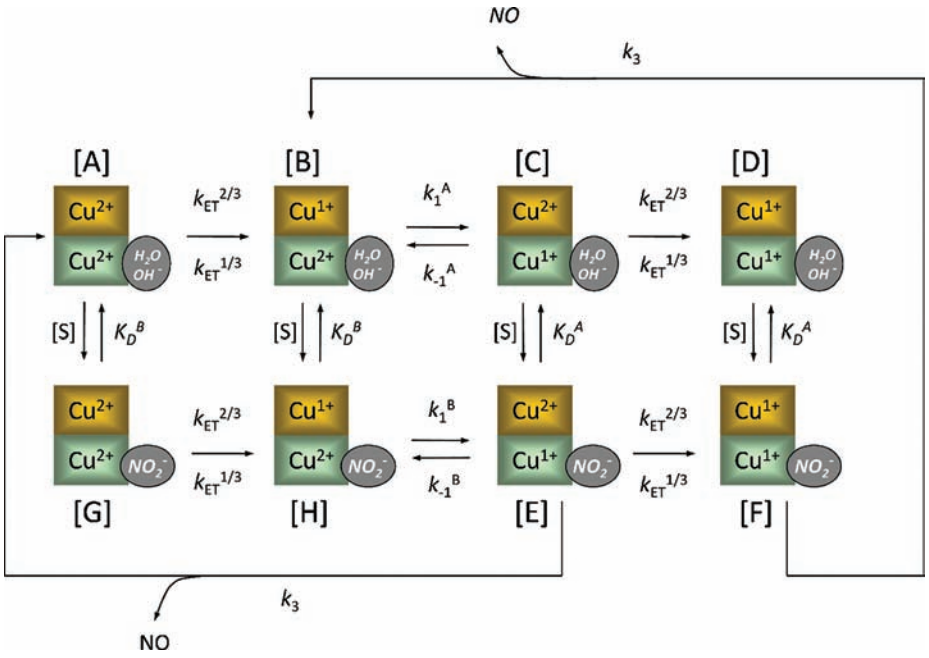

Figure 7. Proposed enzyme mechanism of NiR enzyme immobilized on modified gold electrode. Type-1 copper center is marked yellow, whereas type-2 copper center (active site) is green. The concentration of the enzyme at each possible step of the catalysis is given by [A] − [G]. Top part of the scheme represents low nitrite conditions with water or hydroxyl ion (depending on pH) bound to the active site, whereas the bottom part shows high nitrite conditions with NO_2^- bound to type-2 copper site. The A and B subscripts on intramolecular ET rate (k_1 and k_{-1}) and dissociation constants (K_D) abbreviate routes A and B, respectively. The heterogenic, interfacial electron transfer is abbreviated by $k_{ET}^{1/3}$ and $k_{ET}^{2/3}$. k_{-1}^A and k_{-1}^B are determined using the difference between reduction potentials of the type-1 and type-2 copper sites (ΔE^A and ΔE^B in Table 1) and using the forward ET rates (k_1^A and k_1^B).

Table 1. Effect of pH on Kinetic and Equilibrium Constants of ATTO 565 Labeled L93C Cu-NiR Studied on 6-MH Gold[a]

	pH 5.45	pH 6.85
$k_{ET}^{2/3}$ (s^{-1})	3.8 ± 1.9	3.0 ± 0.4
$k_{ET}^{1/3}$ (s^{-1})	104.8 ± 27.9	70.1 ± 15.2
k_1^A (s^{-1})	2100.0*	24.1 ± 3.3
ΔE^A (mV)	50.0*	0.0*
k_1^B (s^{-1})	10.7 ± 2.4	47.5 ± 4.8
ΔE^B (mV)	0.0*	0.0*
k_3 (s^{-1})	113.4 ± 28.8	113.4*
K_D^A (mM)	0.083 ± 0.013	0.43 ± 0.13
K_D^B (mM)	0.72 ± 0.25	4.84 ± 0.44

[a] The rates and equilibrium constants that were fixed in the fit are indicated by an asterisk.

parameter needs to be fixed in order to obtain a single unique solution. At pH 5.45, k_1^A, ΔE^A, and ΔE^B were fixed as sufficient, and reliable literature values are available for these constants.[8,9,41,42] For pH 6.85, ΔE^A, and ΔE^B were also fixed, but k_1^A was not because of conflicting values in the literature.[22,41,42] Instead, k_3 was fixed to be the same as that obtained at pH 5.45. At high nitrite concentration (>520 μM), the activity of NiR deviates from HMM kinetics (Figure 6A and B black line), which tightly correlates with a substantial change in type-1 copper site oxidation state (Figure 6A′ and B′).

Random Sequential Mechanism (RSM). In the RSM,[8,9] catalysis proceeds via route A at low nitrite concentrations (reduction of the type-2 copper site before NO_2^- binds to the type-2 copper site), which, at high nitrite concentration is diverted to route B (reduction after NO_2^- binding). Here, it is shown that the speed of both routes depends on pH, which is due to changes in intramolecular ET rate (Table 1). Our analysis at pH 5.45 shows a dramatic (>100-fold) decrease in intramolecular ET (k_1^A vs k_1^B, Table 1) when moving from route A to B. This change is directly related to the replacement of the type-2 copper site ligand from H_2O to NO_2^-, which is in agreement with literature reports showing that the intramolecular ET is slower when NO_2^- is bound than when H_2O is bound.[31,41−43] We have tested the model to check if it is possible to change the order of the routes (i.e., route B at low nitrite concentration and route A at high nitrite concentration). This route change (or swap) would occur if $K_D^A > K_D^B$, with concurrently $k_1^A < k_1^B$ in order to fit data. By systematically varying the values of the fixed parameters (see Table 3, Supporting Information), it is shown that at pH 5.45 such a swap is not consistent with the data, and thus, route A (reduction before nitrite binding) dominates at low nitrite concentration, and route B (nitrite-binding-before-reduction) takes over at high nitrite concentration. The same analysis shows that the parameters shown in Table 1 are relatively insensitive to the values of the backward intramolecular ET rates (k_{-1}^A and k_{-1}^B) and that one can only get a reasonable fit with k_1^A between 400 and 5000 s^{-1} and k_1^B between 10 and 40 s^{-1}. In contrast, at high pH (6.85) the two possible scenarios are in principle consistent with our data. In other words, based on the data presented here it is not possible to prove for pH 6.85 that at low nitrite concentration route A dominates, while at high nitrite concentration route B prevails (see Table 3, Supporting Information).

In summary, at pH 5.45, the enzyme predominantly has its type-2 copper site reduced before nitrite binds, but as the nitrite

level increases, NO_2^- ions will bind first, reducing the overall catalytic rate. At pH 6.85 this sequence of events cannot be unambiguously determined. For illustrative purposes, we have chosen to show a set of parameters (Table 1) that is consistent with the low pH data in which route B becomes dominant at high nitrite concentration. The scenario and the parameters shown in Table 1 are those in best agreement with literature. The dependence of substrate binding affinity (K_D^B in Table 1) on pH is similar to that found for K_D^{ox} of NiR from *Alcaligenes xylosoxidans*,[16] *Ax*NiR (in frozen samples $K_D^{ox} \approx 30\ \mu$M at pH 5.2, $K_D^{ox} \approx 350\ \mu$M at pH 7.5) and *A. faecalis*[9] (in frozen samples $K_D^{ox} \approx 1$ mM at pH 6.0, $K_D^{ox} \approx 10$ mM at pH 7.0). Second, the 2-fold increase in intramolecular ET rate at pH 6.85 (k_1^A vs k_1^B in Table 1) shows that ET to the type-2 copper site with OH^- as a ligand is slower than if NO_2^- is coordinating, a fact that is also reported in literature.[12,13,44,45]

Our data thus indicate that the gradual change from route A to route B occurs at nitrite concentrations of ≈520 μM. This means that, up to 520 μM, the type-2 copper site is reduced at a rate k_1^A (Table 1). After switching to route B at higher nitrite concentration, the site will be reduced with rate k_1^B (Table 1). Because at pH 6.85, k_1^B is larger than k_1^A, increasing the nitrite concentration above 520 μM leads to a further oxidation of the type-1 copper site under turnover conditions, and thus, F_i continues to decrease (Figure 6A′). However, the opposite is the case for pH 5.45 (Figure 6B′, $k_1^B < k_1^A$). Similar to F_i, k_{cat} significantly changes above 520 μM NO_2^- too (Figure 6A and B). As a result, the overall kinetics of NiR deviates from the typical HMM behavior.

DISCUSSION

NiR Heterogeneity on Electrode. Based on PFV data, we previously hypothesized that the homotrimeric structure of NiR gives rise to heterogeneous ET rates (k_{ET}) to monomers within the trimer.[8,9] Here, more direct evidence is provided, which confirms that this hypothesis and enables us to quantify the dispersion in k_{ET} (Table 1). At both pH values, two monomers within the trimer have an approximately 25-fold smaller k_{ET} rate than the third monomer (compare $k_{ET}^{1/3}$ to $k_{ET}^{2/3}$ in Table 1). Assuming an exponential ET rate decay value of $\beta = 0.9$ Å^{-1}, this difference in k_{ET} rate corresponds to a 3.6 Å difference in distance.[46,47] This distance illustrates how much further an electron has to travel from the electrode to the type-1 copper site. The relatively small difference in distance indicates that all type-1 copper sites of a trimer face the electrode surface (Figure 1). The enzyme does not bind 'side on', as this would result in at least one monomer being spaced apart from the electrode by more than 35 Å (a distance between type-1 Cu sites taken from NiR crystallographic structure).[10]

Model. Our spectroelectrochemistry data can be only explained by the full model (route A + route B) of Figure 7. In this study we have also constructed models based on either routes A or B only. Neither of these was able to explain two fundamental findings of NiR enzyme catalysis: substrate inhibition at low pH and substrate activation at high pH (Figure 6). Instead, models based on either routes A or B alone resulted in HMM kinetics. Previously, Wijma et al. postulated a RSM to explain the PFV data obtained on carbon electrodes.[8,9] The model was based on various assumptions of interfacial, intramolecular ET rate, and NO_2^- binding kinetics. Here, by using a new fluorescence method we are able to obtain new information on these parameters, which confirm that the overall speed of each route (A and B) is not affected by substrate binding kinetics. Instead it is purely due to a change in NiR's internal ET, which depends on the ligand coordinated to the type-2 active site. Based on the model shown in Figure 7 and pH dependency (Table 1), the internal ET rate to the type-2 copper site decreases with copper ligand in the following order: $H_2O > NO_2^- > OH^-$. This order is consistent to earlier reports.[8,9] Furthermore, the parameters show that all three rates (k_{ET}, k_1, and k_3) influence the overall turnover rate, with k_{ET} exerting the most influence, followed by k_1. Finally, k_3 has the least limiting effect on the turnover rate.

The groups of Hasnain and Scrutton, using NiR from *Ax*NiR, also observed an increase in the catalytic rate at high nitrite concentrations, and they postulated two apparent substrate-binding sites. The authors note that since there is no direct evidence for a second nitrite binding site, the effect may be explained by two nitrite binding affinities.[51] Our results are qualitatively in agreement with this model. Here, the two binding affinities are given by K_D^A and K_D^B, representing the binding of nitrite to the reduced and oxidized type-2 copper, respectively. Laser flash-photolysis experiments for *Ax*NiR showed that for semireduced NiR, the electron distributes between type-1 and type-2 copper sites (according to thermodynamic equilibrium). After nitrite binds to the type-2 copper site, this equilibrium adjusts, fully oxidizing the type-1 copper site and reducing the type-2 copper site. In correspondence with our model, their data show that nitrite binds to the type-2 copper site in both redox states.[52] It is proposed that binding of nitrite to the type-2 copper site increases its reduction potential, increasing the intramolecular ET rate. Here, we propose that this is consistent with the RSM, in which k_1 increases when NO_2^- binds to the active site. We note that in our model, the difference in the reduction potential between the type-1 and type-2 copper site (ΔE^A and ΔE^B) were fixed as they could not be independently determined.

NiR at Rest and During Turnover. Table 1 (see also Table 3, Supporting Information) shows that at pH 5.45, the intramolecular ET to the type-2 copper site without substrate bound is very fast (k_1^A) and diminishes when the enzyme−substrate complex is formed (k_1^B). In contrast, both ET rates at pH 6.85 have similar magnitudes, comparable to the pH 5.45 value when nitrite is bound (i.e., k_1^B). Values obtained at low nitrite concentration are comparable to data obtained with pulse radiolysis experiments from *A. xylosoxidans*,[41−43,48] which show a similar dependence on pH (compare k_1^A from Table 1 to values in Table 2 'no substrate'). Unlike literature values,[41,42] however, it is found that at high nitrite concentration (≥520 μM), the intramolecular ET rate decreases significantly at low pH and slightly increases at high pH (compare k_1^B from Table 1 to Table 2 'with substrate, no turnover'). We speculate that this contradiction arises from

Table 2. Summary of Literature Values of Intramolecular ET Rate between Type-1 and -2 Copper Sites of NiR.[a]

NiR state	pH	k_1 (s^{-1})
no substrate	5.5−6.0	2100[41]
	7.0	450−1800[41−43,48]
with substrate, no turnover	5.5−6.0	2100[41]
	7.0	150−900[41−43,48]
turnover	5.5−6.0	0.024[49]
	7.0	35[22]

[a] Values are obtained at low (5.5−6.0) and high pH (7.0) as well as for different enzyme states.

the fact that our data are measured under NiR turnover, whereas for the pulse radiolysis studies, nonturnover conditions were used.[41,42] Therefore, our data are compared more adequately to data measured under turnover conditions (Table 2 'turnover').[22,49] Using single enzyme studies, it was already found that the internal ET rate in NiR from *A. faecalis* during catalysis is significantly reduced[22] when compared to pulse radiolysis studies.[41−43] Others have found that the ET rate of NiR from *Hyphomicrobium denitrificans* during turnover, at pH 6.0, and high nitrite concentration diminishes almost to 0,[49] in agreement with our data (compare k_1^B from Table 1 to Table 2 'turnover'). In summary, the data presented here and in the literature show that a different set of parameter values applies for NiR during catalysis compared to its resting state. A resting enzyme has a higher intramolecular ET rate that decreases in the presence of nitrite at high pH (7.0), whereas a catalytically active enzyme has a similarly high ET rate only at low pH (5.5−6.0), before nitrite binds to the enzyme's active site. However, once NO_2^- is bound or when the pH increases to ≈7.0, it is observed that the internal ET rate diminishes. This can partly be explained by a change in midpoint potential of the type-2 Cu site upon binding of different ligands (pH rise from 5.5 to 6.0 to 7.0 and lowers it by 80−100 mV).[41,44] However, to account for the difference between the resting and active state, we suggest that the reason for the drop in ET rate during catalysis is the occurrence of an additional rate-limiting step, such as the transport of one or two protons required to complete the enzymatic cycle.

pH-Profile of NiR. The fact that the internal ET rate in NiR is higher at low pH correlates to pH profiles of k_{cat} (Figure 6A and B), suggesting that the intramolecular ET rate determines the overall enzyme activity. Many studies, with pseudoazurin as an electron donor,[11,32] have shown that NiR's enzyme catalytic activity is affected by pH, with approximately 3 times higher activities recorded at low pH = 5.5−6.0 (∼1500−1600 s^{-1}) compared to high pH = 7.0 (∼390 s^{-1}).[4,32] Similar behavior of k_{cat} was found with artificial electron donors, like methylviologen[5] as well as in our PFV studies. Our k_{cat} = 8.9 s^{-1} at pH 6.85 corresponds with V_{max} = 6.5 ± 2 s^{-1} (pH = 7.0) reported for *A. faecalis* NiR (*Af*NiR) linked to a SAM modified glass surface,[22] whereas our k_{cat} = 23 s^{-1} at pH 5.45 is in a good agreement with k_{cat} = 30 s^{-1} (pH = 6.0), as found in electrochemistry experiments on *Ax*NiR immobilized on methyl-benzenethiol SAM modified gold.[50]

Considering similar values for the interfacial ET rate, k_{ET}, and k_3 (Table 1), the pH dependence of k_{cat} is due to changes in intermolecular ET rate (k_1). Studies of Asp98 and His255 mutants of *Af*NiR have suggested that Asp and His residues around the type-2 Cu active site control the ET process by providing protons in an ET coupled protonation step.[14,15] Single and multiple turnover experiments by the groups of Hasnain and Scrutton on *Ax*NiR have confirmed that at pH 7.0, the rate-limiting catalytic step is a single protonation event.[51] In a more recent publication by the same group, the main proton source in *Ax*NiR was identified to be Asn90 (Asn 98 in *Af*NiR), with a much smaller role for His254 (His255 in *Af*NiR).[52] Using kinetic isotope effects, the protonation step was kinetically linked to the intramolecular ET rate (in this manuscript given by k_1).[51]

■ ASSOCIATED CONTENT

Supporting Information. Figure 8 showing details of the spectroelectrochemical cell. Details of rate and equilibrium values obtained when the fixed parameters in Table 1 are systematically varied. The full equations for k_{cat} and F_i based on the model shown in Figure 7 and used to fit the data shown in Figure 6 are also provided. This material is available free of charge via the Internet at http://pubs.acs.org.

■ AUTHOR INFORMATION

Corresponding Author
L.J.C.Jeuken@leeds.ac.uk

■ ACKNOWLEDGMENT

This work was supported by the European Community (FP6) through the Marie Curie Research Training Network "EdRox" (contract no. MRTN-CT-2006-035649).

■ REFERENCES

(1) Adman, E. T.; Murphy, M. E. P. *Handbook of Metalloproteins*; Messerschmidt, A., Huber, R., Wieghardt, K., Poulos, T., Eds.; John Wiley & Sons, Ltd., Chichester, U.K., 2001, 1381.
(2) Kukimoto, M.; Nishiyama, M.; Murphy, M. E.; Turley, S.; Adman, E. T.; Horinouchi, S.; Beppu, T. *Biochemistry* **1994**, *33*, 5246.
(3) Libby, E.; Averill, B. A. *Biochem. Biophys. Res. Commun.* **1992**, *187*, 1529.
(4) Kukimoto, M.; Nishiyama, M.; Tanokura, M.; Adman, E. T.; Horinouchi, S. *J. Biol. Chem.* **1996**, *271*, 13680.
(5) Kakutani, T.; Watanabe, H.; Arima, K.; Beppu, T. *J. Biochem.* **1981**, *89*, 463.
(6) Astier, Y.; Bond, A. M.; Wijma, H. J.; Canters, G. W.; Hill, H. A. O.; Davis, J. J. *Electroanalysis* **2004**, *16*, 1155.
(7) Astier, Y.; Canters, G. W.; Davis, J. J.; Hill, H., A.; Verbeet, M. P.; Wijma, H. J. *ChemPhysChem* **2005**, *6*, 1114.
(8) Wijma, H. J.; Jeuken, L. J.; Verbeet, M. P.; Armstrong, F. A.; Canters, G. W. *J. Am. Chem. Soc.* **2007**, *129*, 8557.
(9) Wijma, H. J.; Jeuken, L. J.; Verbeet, M. P.; Armstrong, F. A.; Canters, G. W. *J. Biol. Chem.* **2006**, *281*, 16340.
(10) Murphy, M. E.; Turley, S.; Adman, E. T. *J. Biol. Chem.* **1997**, *272*, 28455.
(11) Kataoka, K.; Furusawa, H.; Takagi, K.; Yamaguchi, K.; Suzuki, S. *J. Biochem.* **2000**, *127*, 345.
(12) Zhao, Y.; Lukoyanov, D. A.; Toropov, Y. V.; Wu, K.; Shapleigh, J. P.; Scholes, C. P. *Biochemistry* **2002**, *41*, 7464.
(13) Ellis, M. J.; Dodd, F. E.; Strange, R. W.; Prudencio, M.; Sawers, G.; Eady, R. R.; Hasnain, S. S. *Acta Crystallogr., Sect. D: Biol. Crystallogr.* **2001**, *57*, 1110.
(14) Boulanger, M. J.; Kukimoto, M.; Nishiyama, M.; Horinouchi, S.; Murphy, M. E. *J. Biol. Chem.* **2000**, *275*, 23957.
(15) Boulanger, M. J.; Murphy, M. E. *Biochemistry* **2001**, *40*, 9132.
(16) Abraham, Z. H.; Smith, B. E.; Howes, B. D.; Lowe, D. J.; Eady, R. R. *Biochem. J.* **1997**, *324* (Pt 2), 511.
(17) Averill, B. A. *Chem. Rev.* **1996**, *96*, 2951.
(18) Hulse, C. L.; Tiedje, J. M.; Averill, B. A. *J. Am. Chem. Soc.* **1989**, *111*, 2322.
(19) Wasser, I. M.; de Vries, S.; Moenne-Loccoz, P.; Schroder, I.; Karlin, K. D. *Chem. Rev.* **2002**, *102*, 1201.
(20) Adman, E. T.; Godden, J. W.; Turley, S. *J. Biol. Chem.* **1995**, *270*, 27458.
(21) Strange, R. W.; Murphy, L. M.; Dodd, F. E.; Abraham, Z. H.; Eady, R. R.; Smith, B. E.; Hasnain, S. S. *J. Mol. Biol.* **1999**, *287*, 1001.
(22) Kuznetsova, S.; Zauner, G.; Aartsma, T. J.; Engelkamp, H.; Hatzakis, N.; Rowan, A. E.; Nolte, R. J.; Christianen, P. C.; Canters, G. W. *Proc. Natl. Acad. Sci. U.S.A.* **2008**, *105*, 3250.
(23) Kuznetsova, S.; Zauner, G.; Schmauder, R.; Mayboroda, O. A.; Deelder, A. M.; Aartsma, T. J.; Canters, G. W. *Anal. Biochem.* **2006**, *350*, 52.

(24) Salverda, J. M.; Patil, A. V.; Mizzon, G.; Kuznetsova, S.; Zauner, G.; Akkilic, N.; Canters, G. W.; Davis, J. J.; Heering, H. A.; Aartsma, T. J. *Angew. Chem., Int. Ed.* **2010**, *49*, 5776.
(25) Schmauder, R.; Alagaratnam, S.; Chan, C.; Schmidt, T.; Canters, G. W.; Aartsma, T. J. *J. Biol. Inorg. Chem.* **2005**, *10*, 683.
(26) Wijma, H. J.; Boulanger, M. J.; Molon, A.; Fittipaldi, M.; Huber, M.; Murphy, M. E.; Verbeet, M. P.; Canters, G. W. *Biochemistry* **2003**, *42*, 4075.
(27) Jeuken, L. J. C.; Daskalakis, N. N.; Han, X.; Sheikh, K.; Erbe, A.; Bushby, R. J.; Evans, S. D. *Sens. Actuators, B* **2007**, *124*, 501.
(28) Jeuken, L. J. C.; Connell, S. D.; Henderson, P.; Gennis, R. B.; Evans, S. D.; Bushby, R. J. *J. Am. Chem. Soc.* **2006**, *128*, 1711.
(29) Fourmonda, V.; Hokec, K.; Heeringd, H., A.; Bafferet, C.; Lerouxa, F.; Bertranda, P.; Leger, C. *Bioelectrochemistry* **2009**, *76*, 141.
(30) Haung, C. Y. *Methods Enzymol.* **1979**, *63*, 54.
(31) Suzuki, S.; Kataoka, K.; Yamaguchi, K.; Inoue, T.; Kai, Y. Coord. Chem. Rev. **1999**, *190*−*192*, 245.
(32) Wijma, H. J.; Canters, G. W.; de Vries, S.; Verbeet, M. P. *Biochemistry* **2004**, *43*, 10467.
(33) Leger, C.; Bertrand, P. *Chem. Rev.* **2008**, *108*, 2379.
(34) Leger, C.; Jones, A. K.; Albracht, S. P. J.; Armstrong, F. A. *J. Phys. Chem. B* **2002**, *106*, 13058.
(35) Chance, R. R.; Prock, A.; Silbey, R. *Adv. Chem. Phys.* **1978**, *37*, 1.
(36) Lakowicz, J. R. *Principles of Fluorescence Spectroscopy*; Springer: New York, 2004.
(37) Lakowicz, J. R.; Geddes, C. D.; Gryczynski, I.; Malicka, J.; Gryczynski, Z.; Aslan, K.; Lukomska, J.; Matveeva, E.; Zhang, J.; Badugu, R.; Huang, H. *J. Fluoresc.* **2004**, *14* (4), 425.
(38) Enderlein, J. *Chem. Phys.* **1999**, *247*, 1.
(39) Vasilev, K.; Stefani, F., D.; Jacobsen, V.; Knoll, W.; Kreitera, M. *J. Chem. Phys.* **2004**, *120*, 6701.
(40) Vogelsang, J.; Kasper, R.; Steinhauer, C.; Person, B.; Heilemann, M.; Sauer, M.; Tinnefeld, P. *Angew. Chem., Int. Ed.* **2008**, *47*, 5465.
(41) Kobayashi, K.; Tagawa, S.; Deligeer; Suzuki, S. *J. Biochem.* **1999**, *126*, 408.
(42) Suzuki, S.; Deligeer; Yamaguchi, K.; Kataoka, K.; Kobayashi, K.; Tagawa, S.; Kohzuma, T.; Shidara, S.; Iwasaki, H. *J. Biol. Inorg. Chem.* **1997**, *2*, 265.
(43) Suzuki, S.; Kohzuma, T.; Deligeer; Yamaguchi, K.; Nakamura, N.; Shidara, S.; Kobsyashi, K.; Tagawas, S. *J. Am. Chem. Soc.* **1994**, *116*, 11145.
(44) Jacobson, F.; Pistorius, A.; Farkas, D.; De Grip, W.; Hansson, O.; Sjolin, L.; Neutze, R. *J. Biol. Chem.* **2007**, *282*, 6347.
(45) Jacobson, F.; Guo, H.; Olesen, K.; Okvist, M.; Neutze, R.; Sjolin, L. *Acta Crystallogr., Sect. D: Biol. Crystallogr.* **2005**, *61*, 1190.
(46) Chi, Q.; Zhang, J.; Arslan, T.; Borg, L.; Pedersen, G., W.; Christensen, H., E., M.; Nazmudtinov, R., R.; Ulstrup, J. *J. Phys. Chem. B* **2010**, *114*, 5617.
(47) Smalley, J. F.; Finklea, H. O.; Chidsey, C. E. D.; Linford, M. R.; Creager, S. E.; Ferraris, J. P.; Chalfant, K.; Zawodzinsk, T.; Feldberg, O. S. W.; Newton, M. D. *J. Am. Chem. Soc.* **2004**, *125*, 2004.
(48) Farver, O.; Eady, R. R.; Abraham, Z. H.; Pecht, I. *FEBS Lett.* **1998**, *436*, 239.
(49) Deligeer; Fukunaga, R.; Kataoka, K.; Yamaguchi, K.; Kobayashi, K.; Tagawa, S.; Suzuki, S. *J. Inorg. Biochem.* **2002**, *91*, 132.
(50) Chi, Q.; Zhang, J.; Jensen, P. S.; Christensen, H. E.; Ulstrup, J. *Faraday Discuss.* **2006**, *131*, 181.
(51) Brenner, S.; Heyes, D., J.; Hay, S.; Hough, M., A.; Eady, R., R.; Hasnain, S., S; Scrutton, N., S. *J. Biol. Chem.* **2009**, *284*, 25973.
(52) Leferink, N., G., H.; Han, C.; Antonyuk, S., V.; Heyes, D., J.; Rigby, S., E., J.; Hough, M., A.; Eady, R., R.; Scrutton, N., S.; Hasnain, S., S *Biochemistry* **2011**, *50*, 4121.